yellowish aquamarine has been exploited from the pegmatites (source of information from local community).

## 4.3 Beryl

Chibolele Mine located 8 km south-east of Kamena School has been exploited for beryl until February 1998. The pegmatite at Chibolele Mine (see Fig. 2.17a) hosts euhedral crystals of medium to light green, with traces of yellow and colourless beryl. The green variety has average crystals of 3 cm across and 20 cm long. Numerous other pegmatites in the Masola area host beryl of varying qualities (Figs. 4.2 a and b).

## 4.4 Feldspar and Mica

Feldspar and mica are abundant in most pegmatites of the Kaseba-Katota area. Feldspar occurs as large crystals up to 60 cm in diameter. In deeply weathered pegmatites, feldspar is weathered to kaolin. Mica (Fig. 4.2c) often occurs as thick books measuring 15 cm x 10 cm x 5 cm, commonly associated with feldspar.

## 4.5 Tourmaline

Green tourmaline has been reported in some pegmatites south of Katota School whereas black tourmaline (Figs. 4.2d and e) occurs in Kaseba area southwest of Panswa hills (see Fig.1.1). Black tourmaline is common in pegmatites hosting beryl and aquamarine. It also occurs as thin pencil-like aggregates in the schists north of the study area.


Fig. 4.2: a) Euhedral crystals of aquamarine from a pegmatite at Panswa hills (Fig 1.1). The aquamarine is heavily fractured and cloudy. Marker is 13 cm long. b) Grains of beryl mined from a pegmatite in Masola area (Fig 1.1). The pieces have been broken from a large fractured crystal. Pencil is 15 cm long. c) Mica flakes left after exploitation of aquamarine in a pegmatite, 2 km southeast of Kamena School (Fig 1.1). Camera is 12cm long. d) Weathered black tourmaline in a quarry wall in Kaseba area. Knife is 5cm long. e) Sub– to euhedral crystals of black tourmaline from Panswa hills. Marker is 13 cm long. f) Euhedral transparent crystals of quartz from White Rock Mine, ready for transportation to the market. Compass is 16cm long.

## 4.6 *Quartz*

Euhedral transparent crystals of quartz ranging from 0.5 cm to 6 cm across and from 1 cm to 20 cm long (see Fig. 4.2f) are mined at White Rock Mine about 8 km east of Kamena School. The pegmatite hosting the quartz intrudes the micaceous quartzite, in the form of a stock-work, near its contact with the schist. The quartz crystals are concentrated in irregular 'pockets'. In the centre of the 'pockets' the quartz crystals are embedded in a loose mixture of muscovite, feldspar and lateritic material.

## 4.7 Iron Ore

Iron ore occurs in a deposit about 2 km east of Kamena School in the schists and quartzites. It has been reported that chalcopyrite occurs as disseminations in the dolerite and gabbroic bodies, but is only of academic interest. Guernsey (1951) recorded copper near the source of Mamba River on the border of the Kanona-Serenje sheets.

CHAPTER

5

# 5.0 APPLICATION OF REMOTE SENSING IN THE KASEBA-KATOTA AREA

A Landsat TM image of the area (Fig. 5.1) dated August 1998 was introduced and several aerial photos dated 1981 and 1991 assisted in visualising the geologic units and terrain in the area.

One of the geologic features that shows up strikingly in the Landsat TM image is the structure of crustal rocks such as faults and folds. Some lithological units such as those around Sasa Dome, Kanona and Kaseba-Katota areas (see Fig. 3.1) tend to stand out because of different erosional properties which leave the more resistant layers as ridges rising above the more easily eroded units. Faults, folds and linear structures as seen in the field are compared with those observed from satellite images and aerial photographs for a complete interpretation.

## 5.1 Geological Image Interpretation

### 5.1.1 General

Landsat TM satellite images and aerial photographs are widely used today for identifying and mapping structural features such as faults and folds, drainage patterns and lithological

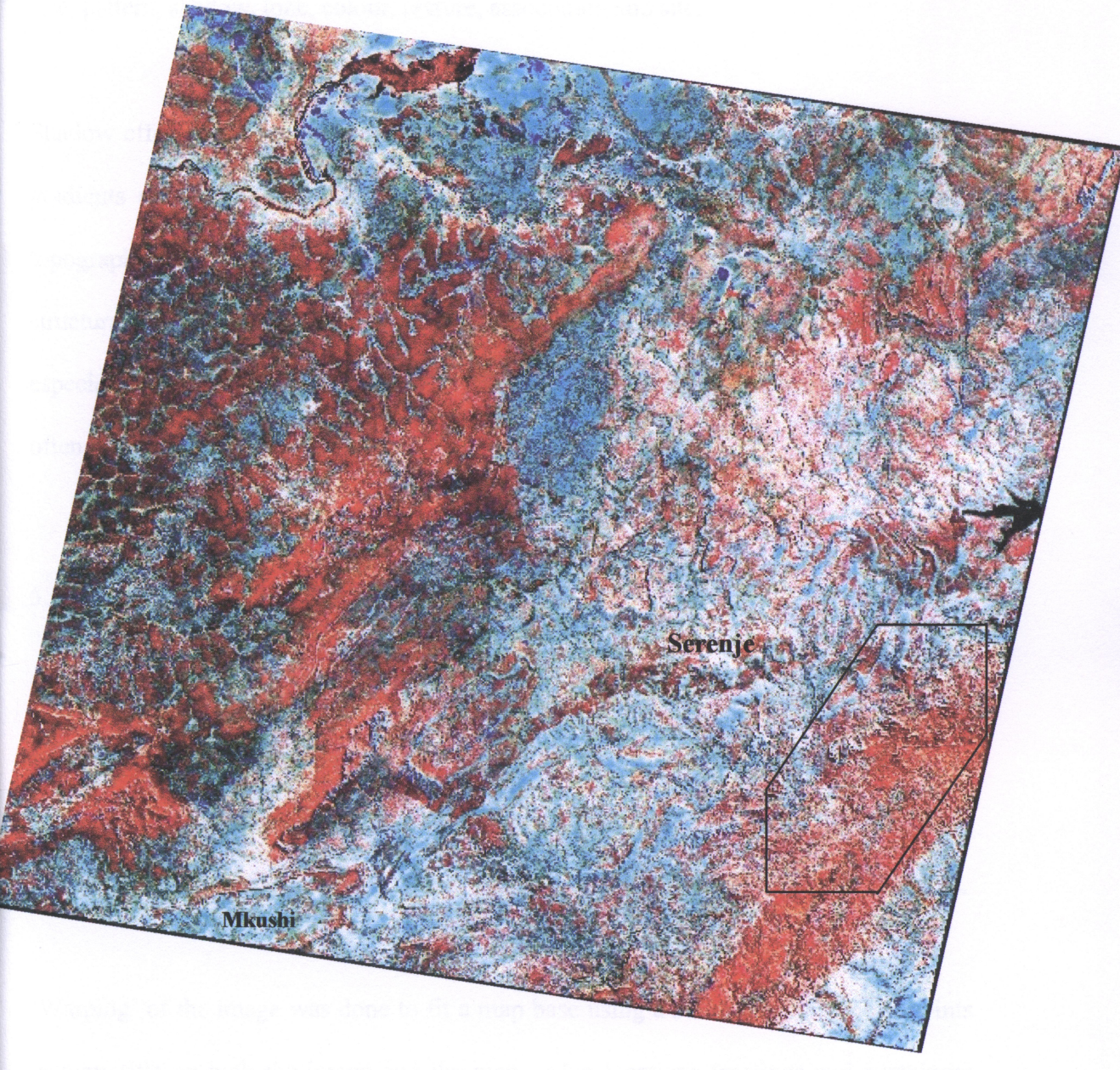


Fig. 5.1: Landsat Thematic Mapper image of Mkushi-Serenje area, dated November 1998. Image bands 4, 5 and 7 are loaded in channels red, green and blue respectively, with equallisation enhancement. The image size is 180 x 185 km. The black box outlines the Kaseba-Katota area. See also Fig. 3.1;

units (Clive, 1990). The geologic interpretation of satellite images and aerial photographs is based on the fundamental recognition of elements that include shape, size, pattern, shadow, tone, colour, texture, association and site.

Shadow effects that are common in mountainous areas and abrupt changes in surface gradients are often helpful in lithological and structural mapping. Shadows enhance topographic and large morphologic features. Vegetation patterns provide clues on structural and lithological changes. However, vegetation remains a limiting factor especially when rock discrimination is attempted on the basis of spectral features. It often hinders and even obstructs direct lithological mapping.

### 5.1.2 Geometric Corrections

Although satellite images provide a relatively distortion-free view of the earth, they do contain both systematic and non-systematic geometric distortions which may need to be corrected. Landsat Thematic Mapper image covering Mkushi and Serenje districts, dated August 1998, was radiometrically corrected and geographically registered (see Fig. 5.1).

'Warping' of the image was done to fit a map base using a set of ground control points recognisable on both the image and the map. Map locations (eastings and northings) were entered automatically via the digitising table. Corresponding screen locations such as river confluences and road junctions were identified using the cursor and automatically recorded in pixel co-ordinates (sample and line). During warping, the program determines polynomial equations to convert original pixel locations to new

locations. By providing information on the map projection, the image was geo-referenced to the given map projection (see Fig. 5.1).

The Kaseba-Katota area was extracted from the scene for study. Bands 4, 5 and 7 (Figs. 5.2a, b and c respectively) were overlaid to make a colour composite to be used as the basis for image interpretation, because it gave the best combination for geological interpretation.

### 5.1.3 Sub-area and Spectral Band Selection

When evaluating the information content of the data, each spectral band was viewed in turn (using a simple linear stretch) to decide on its relative geological information content. This was mainly determined qualitatively by comparing bands with one another and with geological maps.

The selection of three bands for a colour composite simply involved a choice between the NIR band 7 and mid infrared, i.e. 7-5-4 in red, green and blue (RGB) (Fig. 5.2d). For seven-band Landsat TM imagery it can be helpful to calculate the statistics of the image, including the correlation matrix. In theory, pairs of bands showing the lowest correlation and the highest individual variances make the best colour composites, since such combinations possess less duplication of information. Various false colour composites were displayed and compared. Useful combinations for Landsat TM data displayed were 4-5-7 and 4-5-1 in RGB respectively. Selection of the 'best' combination was highly scene dependent (Fig. 5.2d).

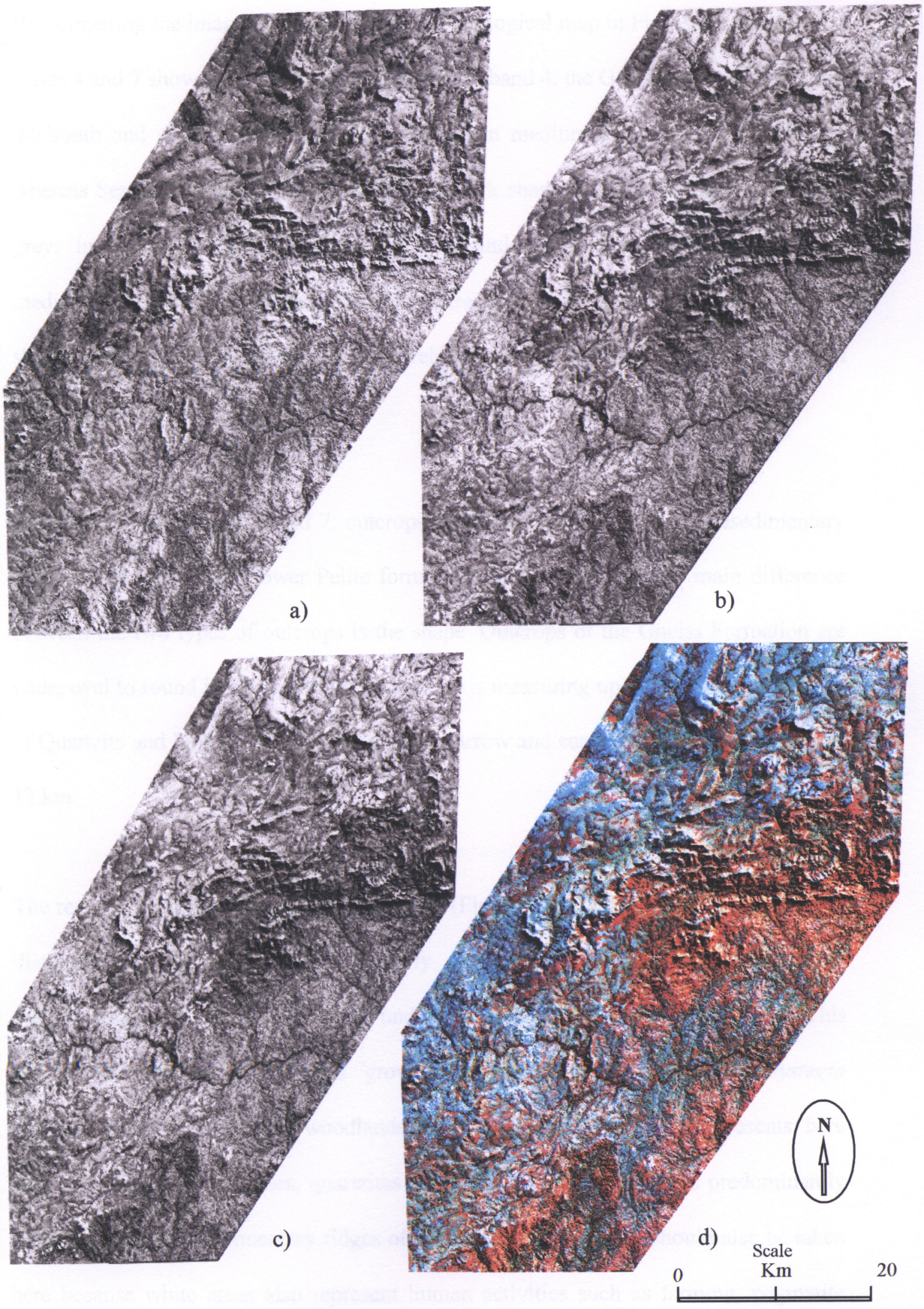


Fig. 5.2: a) TM band 4 with equallisation. b) TM band 5 with equallisation. c) TM band 7 with equallisation. d) False colour composite of TM image of the Kaseba-Katota area. Bands 4, 5 and 7 in channels red, green and blue respectively. Red areas are generally underlain by the Gneiss Group and covered by thickly vegetated woodlands. White generally represents bare outcrops of granites, gneisses, quartzites and schists. Blue areas are characterised by short and mixed vegetation with limited undergrowth and pale brown soils.

By comparing the images in Fig. 5.2, with the geological map in Fig. 2.1, it is clear that bands 4 and 7 show the greatest tonal contrasts. In band 4, the Gneiss Group (Table 1) in the south and south-east of the image appears in medium to bright shades of grey, whereas Serenje Group appears in medium to dark shades of grey and also in whitish grey. In band 7, the Gneiss Group in the south and south-east of the image appears in medium to dark shades of grey, whereas Serenje Group mostly appears in brighter shades of grey. Band 5 shows a high correlation with band 7 with slight variations in their tones.

However, in both bands 4 and 7, outcrops of Gneiss Formation and metasedimentary ridges of Quartzite and Lower Pelite formations appear whitish. The main difference between the two types of outcrops is the shape. Outcrops of the Gneiss Formation are wide, oval to round in shape with the longest axis measuring up to 800m whereas those of Quartzite and Lower Pelite formations are narrow and can be traced continuously for 12 km.

The resulting colour composite image clearly (Fig. 5.2d) brings out different colours to distinguish features that were not easily recognisable such as thickly vegetated woodlands in red. The Gneiss Group underlies most of the areas with red tones. This means that the group supports growth of *Isoberlinia paniculata-Brachystegia* woodlands, which are taller woodlands (see Section 1.5.1). White represents bare outcrops of granites, gneisses, quartzites and schists. The white tone is predominantly represented by metasedimentary ridges of the Serenje Group. Care should also be taken here because white areas also represent human activities such as farming, pegmatite trenching (see Fig. 4.1) and other features such as football pitches at schools, villages or

along and near the road connecting Chisomo Village to Serenje Town (see Figs. 1.0 and 1.1). At the spatial resolution of Kaseba-Katota image, these activities cannot be distinguished.

Light blue represents areas covered by thin plateau soils and sparsely vegetated areas (*Monotones, Protea and Uapaca*). Blue areas are characterised by short and mixed vegetation with limited undergrowth and pale brown soils. This characteristic colour is common in all formations in the area.

### 5.1.4 Image Classification

Classification is the process of sub-dividing a scene into categories based on their spectral characteristics across several bands. This is done by re-assigning each pixel in an image to a class based on its digital number (DN values) in all bands according to a series of pre-defined numerical decision rules. Classification was performed on multi-band images and on derived data sets of processed images, using Image Works (and extension of PCI Image-Works Version 7 software (2000). The aim of classification was to define a series of classes corresponding to spectrally discrete surface materials including granitic intrusions, excavations of pegmatites and sharp lithological boundaries. Both 'unsupervised' and 'supervised' classifications were carried out and the results compared.

In unsupervised classification Fig. 5.3a, the program automatically defined classes based on natural Groupings identified within the ***n*** dimensional spectral distribution of the data. As far as possible, each pixel in the image was assigned to one of these classes whereas

any ambiguous pixels were left unclassified. This process is not guided by prior knowledge of the area, and the classes selected by the computer do not always relate to recognisable surface categories. This process was, however, useful as an initial exploration of the structure of the data. The results of the unsupervised classification were correlated with the geological map (see Fig. 2.1) and aerial photographs. From this correlation, red colour in the classified image represents areas covered by *Isoberlinia paniculata-Brachystegia* woodlands, which are mainly underlain by the Gneiss Formation (see Table 1 and Fig. 2.1). Yellow represents areas covered by *Monotones, Protea and Uapaca* growing sparsely on thin plateau soils and along joints on bare outcrops of granites, gneisses, quartzites and schists. To the south-west of Fig. 5.3a, yellow also represents human settlements, farming activities and excavation. Green represents a mixture of spatial classes low-lying areas with little or no outcrops. To the west of the classified image, green is underlain by granite (compare with Fig. 2.1). Black represents water, moist areas and shadow casts on steep slopes. The unsupervised classification was then used for ground truthing which led to simplification and generation of the supervised classification in Fig. 5.3b.

In supervised classification (see Fig. 5.3b), training areas were decided by interactively defining a series of regions of interest on the screen based on knowledge of the area from fieldwork. Its classification accuracy is an estimated 66%; that is, the spatial information is correctly identified over at least that percentage of surface exposures. There can be considerable subjectivity in setting up and interpreting any classification as was the case in this supervised classification, leading to modified results, which were aimed at reducing the number of classes to four (see Fig. 5.3b). In the supervised image, brown shows areas with pegmatites and/or quarries, black

shows areas with high likelihood of pegmatite occurrence, green represents gneissic terrains, water, moist areas and shadow casts on steep slopes. Yellowish brown represents metasedimentary ridges, bare granitic outcrops and thin soils with very scanty vegetation.

### 5.1.5 Lineament Analysis

When locating lineaments from the remotely sensed, the following characteristic features were considered:

a) sudden shifts or deflection of drainage courses and/or long straight stream channels
b) straight valleys in hard rock areas
c) linear alignments of natural vegetation
d) linear features crossing drainage channels
e) Abrupt topographic discontinuities of landforms, scarps or cliffs and distinct tonal changes on opposite sides of the scarps.
f) Layers of different types and ages of rock units sit side-by-side

Lineament analysis is used to interpret regional structure, to aid in locating buried structures and to map fractures. The analysis was directed towards detection of basement structures, primarily faults. Band 7 of the radiometrically corrected and geographically registered Landsat TM image (Fig. 5.4a) along with aerial photographs were selected for further study. The four selected areas in (Fig. 5.4a) correspond to these in Figs. 5.4b, c, d and e) respectively, showing more details that are

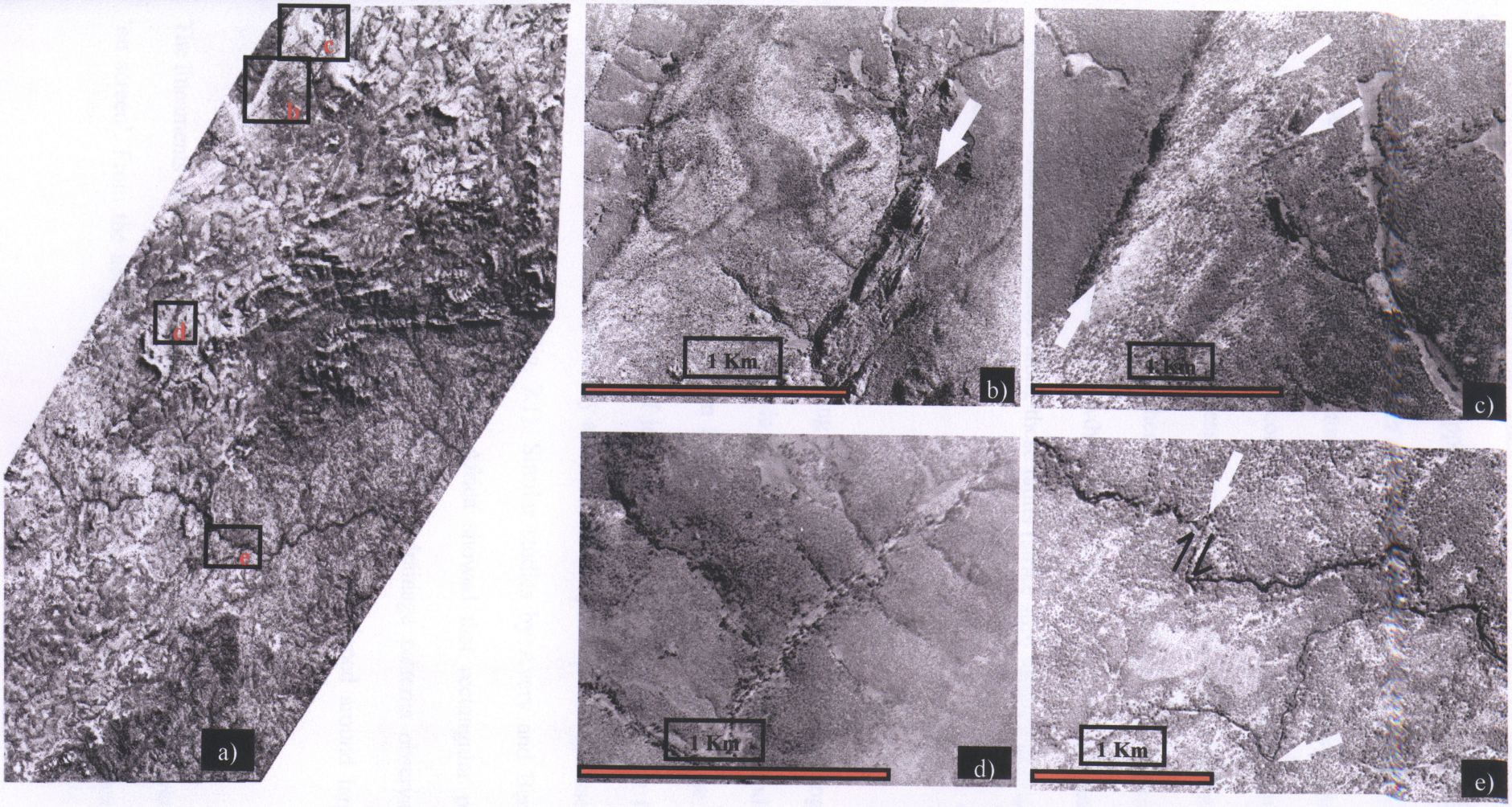


Fig. 5.4: a) TM satellite image band 7 of the Kaseba-Katota area. The red boxes represent areas shown on aerial photographs in b, c, d and e. b) Aerial photograph showing topographic scarps and tonal changes on opposite sides of lineaments in Chitema hills (see arrow). c) Aerial photograph showing linear alignment of vegetation in Chitema Hills (see arrows). d) Aerial photograph showing rectangular drainage pattern of Kansoso River basin. e) Aerial photograph showing deflected rivers around Lukusashi and Fukwe river confluence.

not apparent in the satellite image. These linear features shown by the arrow in Fig. 5.4b represent quartzites in Fig. 2.1 and appear yellow in Fig. 5.3a. In Figs. 5.4c, d and e, the drainage and vegetation pattern reflect the fault systems in the study area. It is clear from these selected areas that linear features correspond to topographic features such as valleys and scarps, whereas others correspond to mappable geologic features such as faults. Faults, as zones of weakness may influence the emplacement of igneous intrusions and therefore localising them. Development of soil and collection of water along these faults has enhanced growth of vegetation, which shows as linear features in Fig. 5.4c. Relative movement along these faults (strike slip) resulted in displacement or deviation of rivers (see Fig. 5.4e).

The type of drainage pattern prevailing in the Kaseba-Katota area is rectangular pattern (see Fig. 5.4d). Rectangular pattern is a variation of dendritic pattern and consists of tributaries that join the main stream at approximately right angles. The rectangular pattern reflects a regional pattern of joints or faults and foliation. From the Kaseba-Katota area, this pattern is typified by areas underlain by schists and gneisses (compare with corresponding areas in Fig. 2.1). Similar studies by Avery and Berlin (1985); Lavreau and Bardinet (1988) in East Africa showed that rectangular patterns are common in schist and gneissic terrains. Other drainage patterns observable in the Kaseba-Katota area are annular patterns. These are developed around large granitic intrusions.

The lineaments interpreted from the satellite image and aerial photographs were digitised 'on screen'. From the aerial photographs and TM image covering the Kaseba-Katota

area, metasedimentary ridges and other linear features show a consistent pattern striking N and NE (see Fig. 5.4a). The most resistant rocks occupy higher elevations, with quartzites forming prominent ridges. Competent rocks of granites and gneisses occasionally emerge as discontinuous strike ridges above the ground. Shaded relief and directional filtering enhanced the appearance of these topographic features and also brought out subdued features such as faults and folds.

*5.1.5.1 Image Enhancement*

The goal of image enhancement was to improve the detectability of objects and patterns for visual interpretation. Much benefit was achieved from contrast stretching edge enhancements and high-frequency filtering through the image. Different high-pass add-back filters were tested on the sub-scene (Sabins, 1996; Greenbaum and Amos, 1998.). Good results were obtained using Laplacian filter such as shown in edge filtered band 7 (Fig. 5.5). The edge-enhanced image was contrast stretched to extract the maximum information from the data. Ideally, tests were carried out on a representative portion of the image using different stretches, and the Look Up Table (LUT) in a NE-SW direction using a 3X3 Kernel Matrix was saved. This was then applied to the image coverage as a whole. Major lineaments and folds were enhanced (see arrows in Fig. 5.5) while the rest of the terrain was suppressed (compare with Fig. 5.4). The enhanced image was used for automatic lineament extraction.

*5.1.5.2 Shaded Relief Model*

Shaded view of relief generally enhances the realism of the terrain. Studies by Lundén et al, 1993 have demonstrated the usefulness of shaded relief images for analysis of

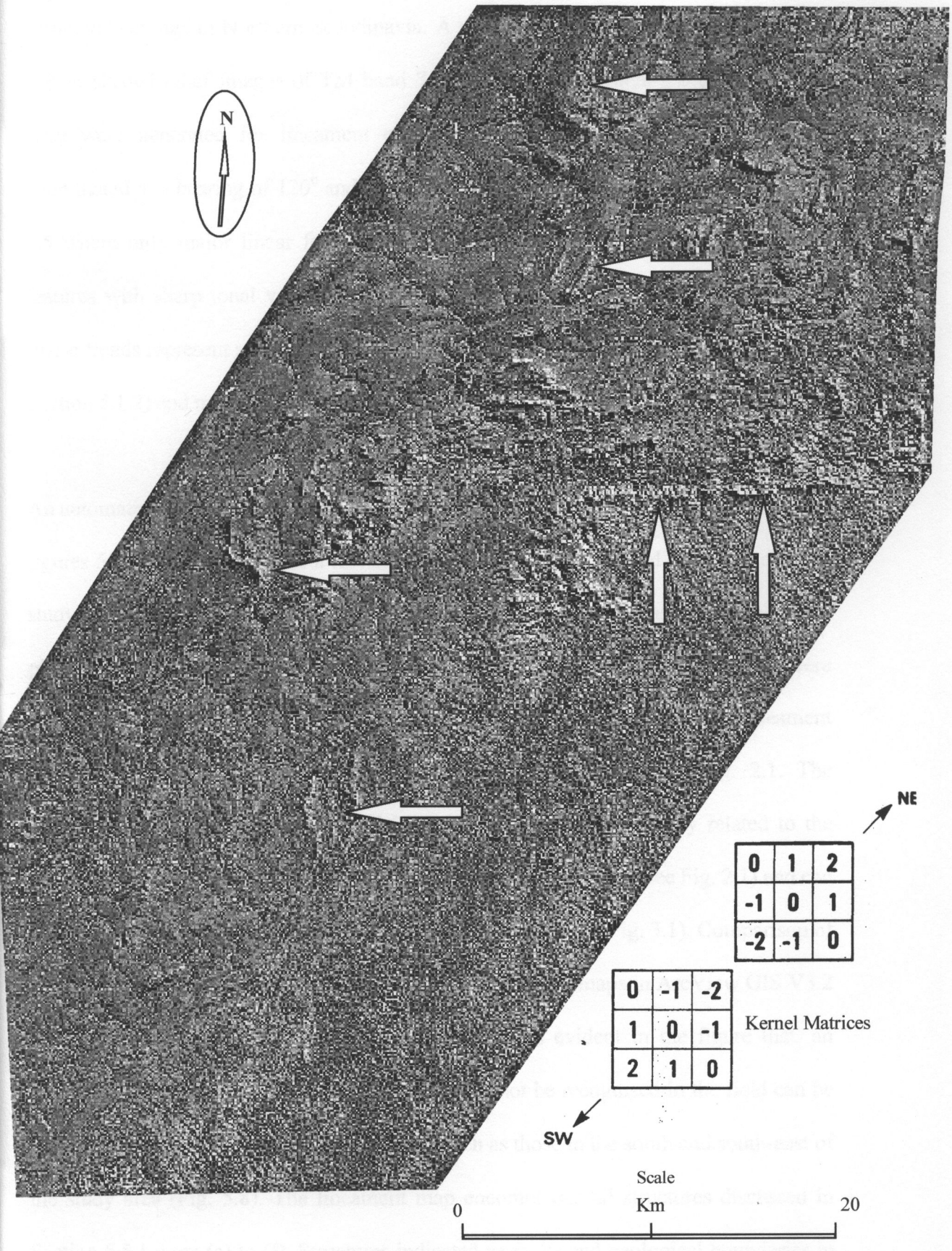


Fig. 5.5: Edge filtered band 7 in NE—SW direction using 3X3 Kernel Matrices shown on the bottom right of the image. Major linear structures of metasedimentary ridges (see arrows) have been enhanced for better detectability. Compare with Fig. 5.2c and Fig. 5.4a.

structural settings in Northern Scandinavia. A similar approach was taken in this study where shaded relief images of TM band 7 with different illuminations over the study area were generated for lineament extraction. Fig. 5.6 is a shaded relief image illuminated at a bearing of 120° and inclination of –30°. Unlike in edge filtering of Fig. 5.5 where only major linear features were enhanced, shaded relief has enhanced all features with sharp tonal variations. Arrows show the prominent trends in the image. These trends represent structural features such as faults and folds, drainage patterns (see Section 5.1.2) and metasedimentary ridges.

An automatic lineament extraction operation was then applied to the enhanced images of figures 5.5 and 5.6 to generate a lineament map showing the general appearance of the study area (Fig. 5.7). The thresh-hold of detection of a lineament was set to 3 pixels (1 pixel = 28m) in order to detect lineaments from that scale. Insignificant features were dissolved and only important ones were retained and shown in Fig. 5.8. The lineament interpretation (Fig. 5.8) was compared with the geological map in Fig. 2.1. The comparison showed that the extracted lineaments in Fig. 5.8 are easily related to the lithological units, faults, and lineaments in the Kaseba-Katota area (see Fig. 2.1) and can be correlated to the adjacent areas of Kanona and Chisomo (see Fig. 3.1). Comparison of Figs. 2.1, 5.2d and 5.8 was done by overlaying the different maps in ArcView GIS V3.2 (2000). The overlays are shown in Fig. 5.9. and it is evident in the figure that, an unlimited amount of lineaments most of which cannot be recognised in the field can be generated from a Landsat TM satellite image such as those in the south and south-east of the study area (Fig. 5.8). The lineament map encompasses all structures discussed in Section 5.5.1 parts (a) to (f). Structures indicated as faults and geological boundaries in the figure, are those proven in the field during mapping and ground truthing.

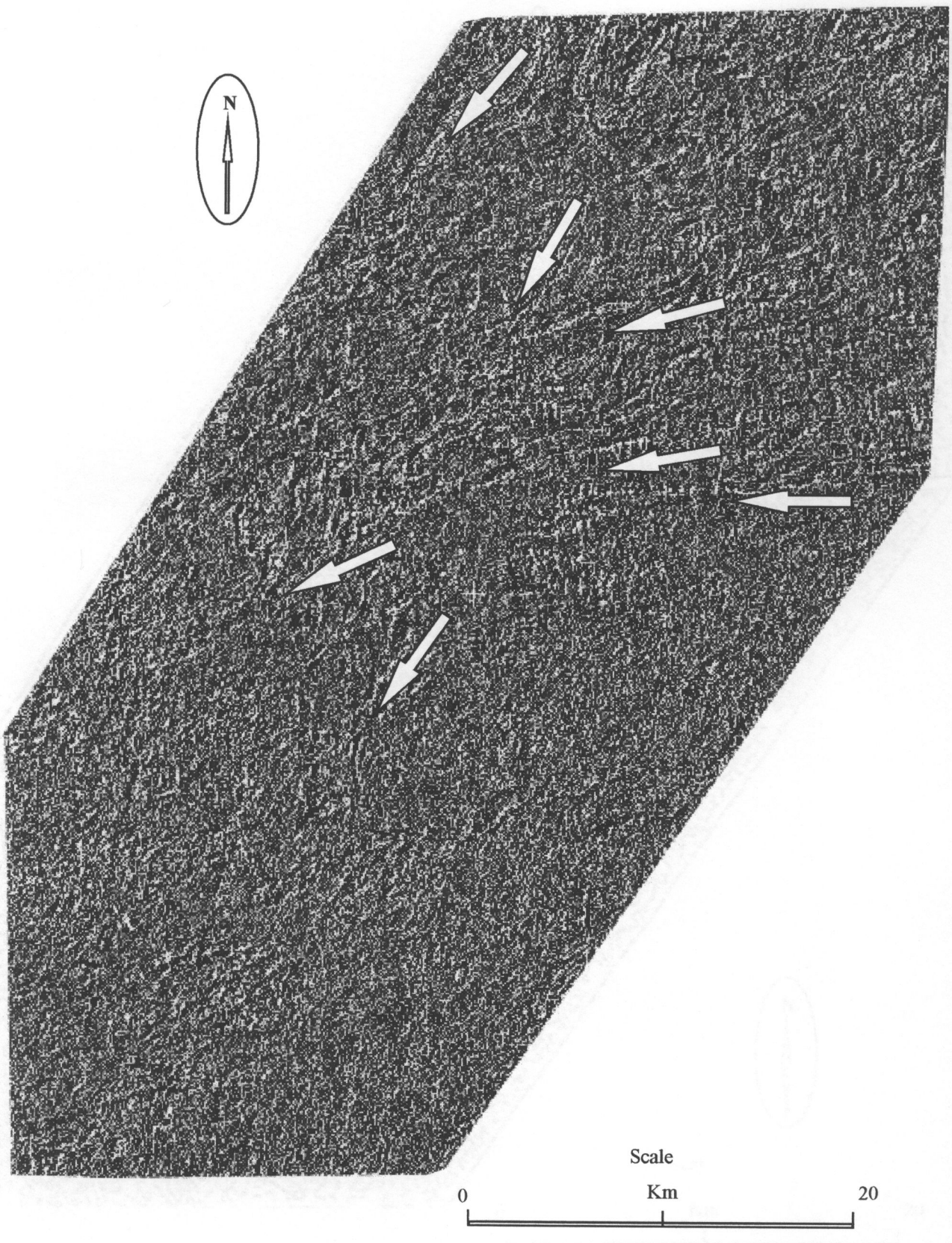


Fig. 5.6: Shaded relief image of band 7 of Kaseba-Katota area. The image is illuminated at a bearing of 120° and inclination of –30°. Arrows indicate the orientation of faults, folds and metasedimentary ridges.

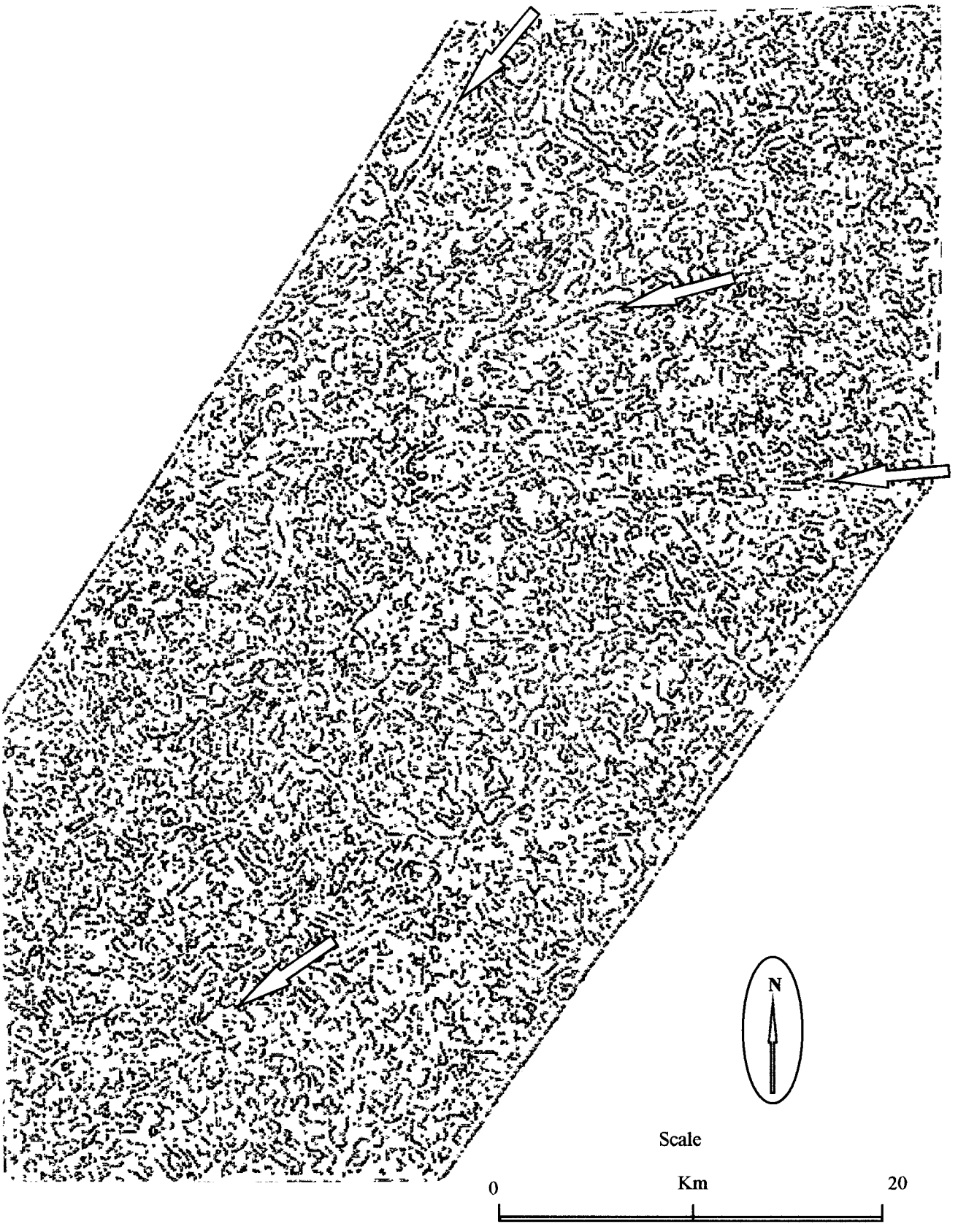


Fig. 5.7: Lineament map of the study area resulting from an automatic lineament extraction using PCI Xpace program, an extension of PCI Image-Works. Major lineaments are easily recognisable (see arrows), but minor ones are dificult to distinguish. However, this map gives a general picture of the study area. A refined lineament map is shown in Fig. 5.8.

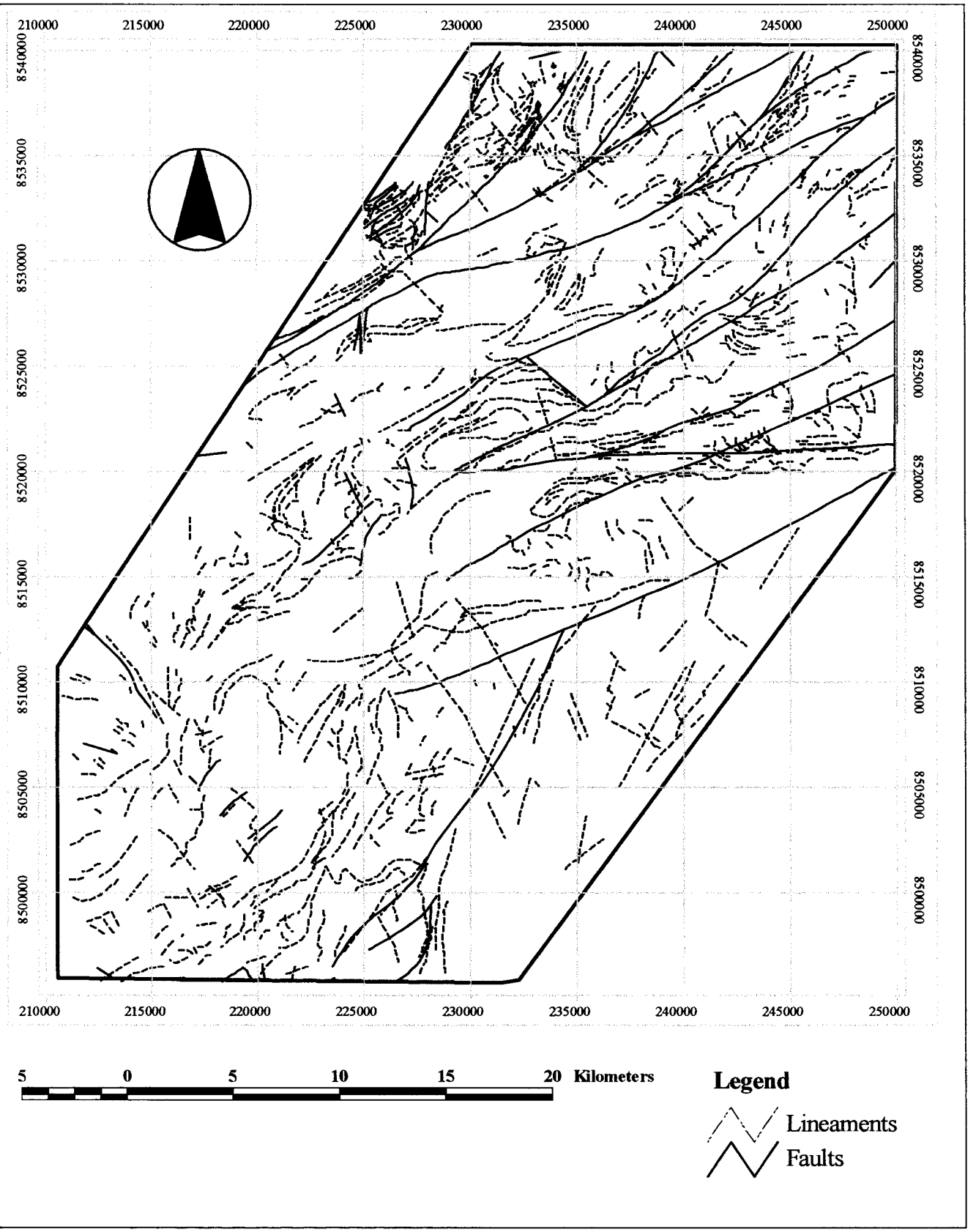


Fig. 5.8: Lineament map of the Kaseba-Katota area resulting from a combination of on-screen digitization (in ArcView GIS environment) of Figs. 5.5 and 5.6 and simplification of Fig. 7. The NE-trending lineaments are related to the Irumide Orogeny whereas the NW-trending lineaments are related to the Pan-African Orogeny (see section 3.2).

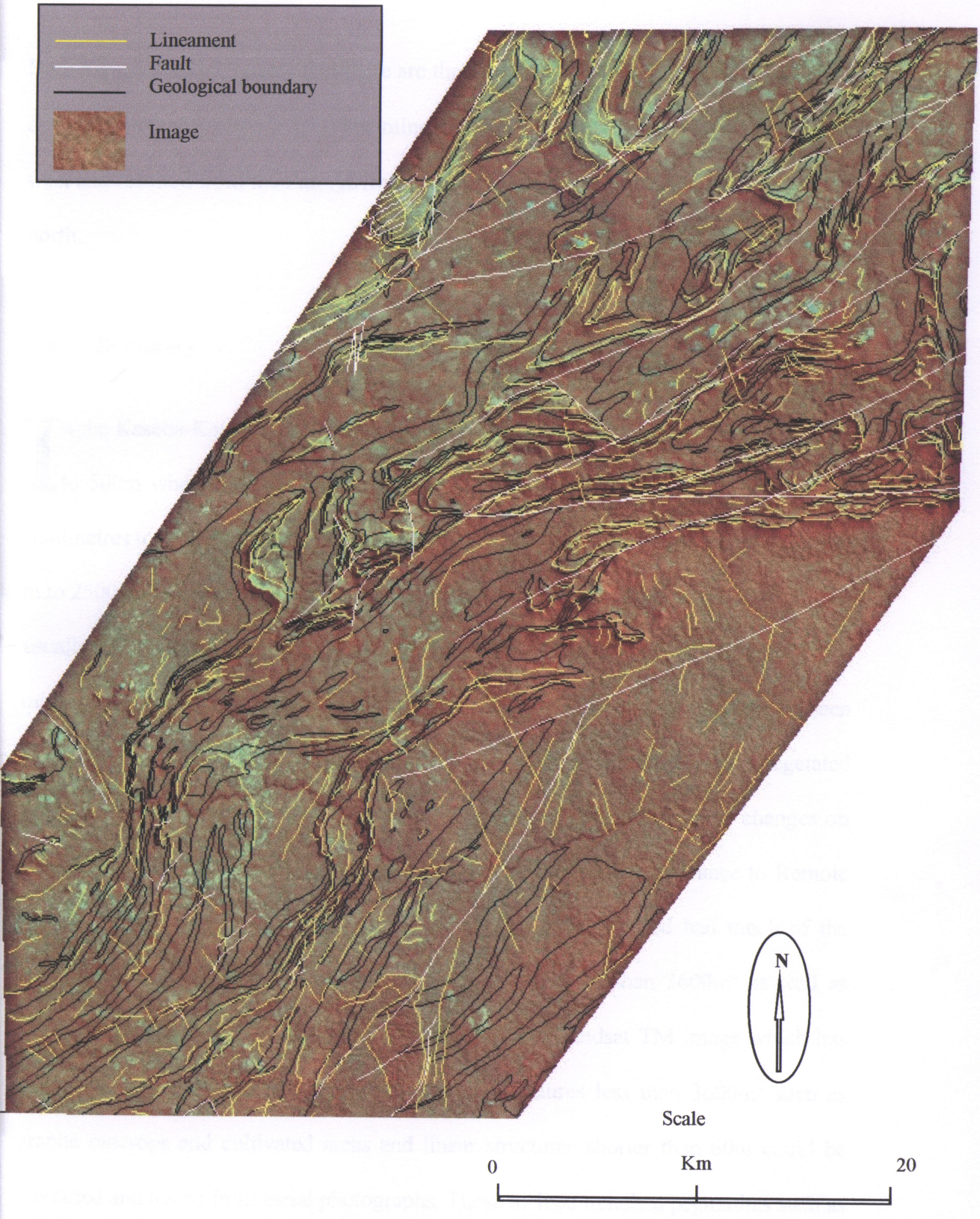


Fig. 5.9: Lineaments, faults and geological boundaries superimposed on a false colour composite image of the Kaseba-Katota area.

lineaments is more conspicuous and trends north-east. This set is a result of the Irumide

Both Figs. 5.8 and 5.9 show that there are three sets of lineaments. The major set of deformation (see Section 3.2.1). The minor set is less conspicuous and trends north-west and resulted from the Pan-African Orogeny. The tertiary set of lineaments trends north.

## 5.2 Summary

In the Kaseba-Katota area, granite and gneiss outcrops range from a few centimetres to 500m whereas those of schists, quartzites and metasiltstones range from a few centimetres to 220m. Structural features such as faults and folds can be traced from 100 m to 2500m. The pegmatites range from 10m to 50m in length, 0.1m to 6m in width and usually form small ridges rising above the general surrounding to about 6 m high. Old mining areas such as Chibolele Mine (see Fig. 2.12a), where vegetation has either been cleared or covered by soil from the excavations, cover about 10000 $m^2$. In non-vegetated areas, all spatial features greater than 900$m^2$ or 60m long with sharp tonal changes on either side could be identified. Though vegetation is the greatest hindrance to Remote Sensing (see Fig. 1.3c), the August 1998 Landsat TM image used had much of the vegetation dry and hence outcrops and mining areas greater than 3600$m^2$ as well as structures greater than 60m long could be seen on this Landsat TM image which has spatial resolution of 28 x 28 m on the ground. Structures less than 3600$m^2$ such as granite outcrops and cultivated areas and linear structures shorter than 60m could be identified and traced from aerial photographs. These include trenched pegmatites such as those around Katota and Masola (see Fig. 4.1) areas, which appear white on the

photographs due to exposure of the quartz-rich pegmatite core and muscovite flakes. However, thickly vegetated areas concealed most of this information on the remotely sensed data. Since almost all the pegmatites are shorter than 60m, direct mapping by use of the Landsat TM image was not possible. But through mapping of lineaments, and faults from the Landsat TM image and strike, joints and foliation from the field, and integration of the two data types, it was possible to map and understand the nature of the pegmatites.

CHAPTER

6

# 6.0 GIS ANALYSIS AND DATA INTERGRATION

## 6.1 General

To further map the lineaments and pegmatites, Geographic Information Systems (GIS) technique was applied. The application of GIS also assisted in bringing together many types of spatial data for an informed decision.

## 6.2 GIS Analysis

Three major stages constituted the GIS analysis. The first stage was to bring all appropriate data together into the database. The second stage was to manipulate the data to extract and derive information relevant to the study. The third stage was the integration of the derived information followed by output.

The first stage involved establishment of spatial extents of the study area, assembling data in digital form and registration of the data into a working projection. The data sources were geological maps of Serenje, Kanona and Chisomo areas (see Fig. 2.1). The maps were digitised and transformed into the working projection. Digitised data included topographic data, drainage data, geological data (rock types and faults), communication network and distribution of human activities. Relevant data derived from image

processing was imported into the GIS database. The data set from image processing included lineaments and land cover classifications.

The second stage was to process the input data in order to extract information for pegmatite mapping. Lineaments, faults and lithological boundaries are significant for pegmatite mapping. These linear features were selected and buffered to produce proximity maps because emplacement of pegmatites shows a spatial association with these lineaments. The proximity maps (buffers) provide an area within which all structurally controlled pegmatites can be located. Faults were buffered for 500m, lineaments for 300m and geological boundaries for 50m (Fig 6.1). The buffer distances were arbitrarily chosen but it puts into account the error of 50m in the eastings and 100m in the northings, resulting from image geocorrection. Spatial analysis was applied to the pegmatites to extract potential areas for gemstone exploration (Fig. 6.2). In this figure, pegmatites intersecting lineaments and faults (green and orange respectively) are economically important as the majority host gemstones. The orientations of pegmatites in the Kaseba – Katota area were also grouped in small domains for statistical analysis. Variations in the orientations of the pegmatites were represented by rose diagrams (cf. Woldai, 1995) and stereo plots. The rose diagrams define differently oriented sets of pegmatites. A class interval of $10^{o}$ azimuth was arbitrary applied as the main division to construct the rose diagrams. Construction of rose diagrams was also based on the type of lithologies in which they occur. Lithological units, that host the pegmatites were classified and buffered.

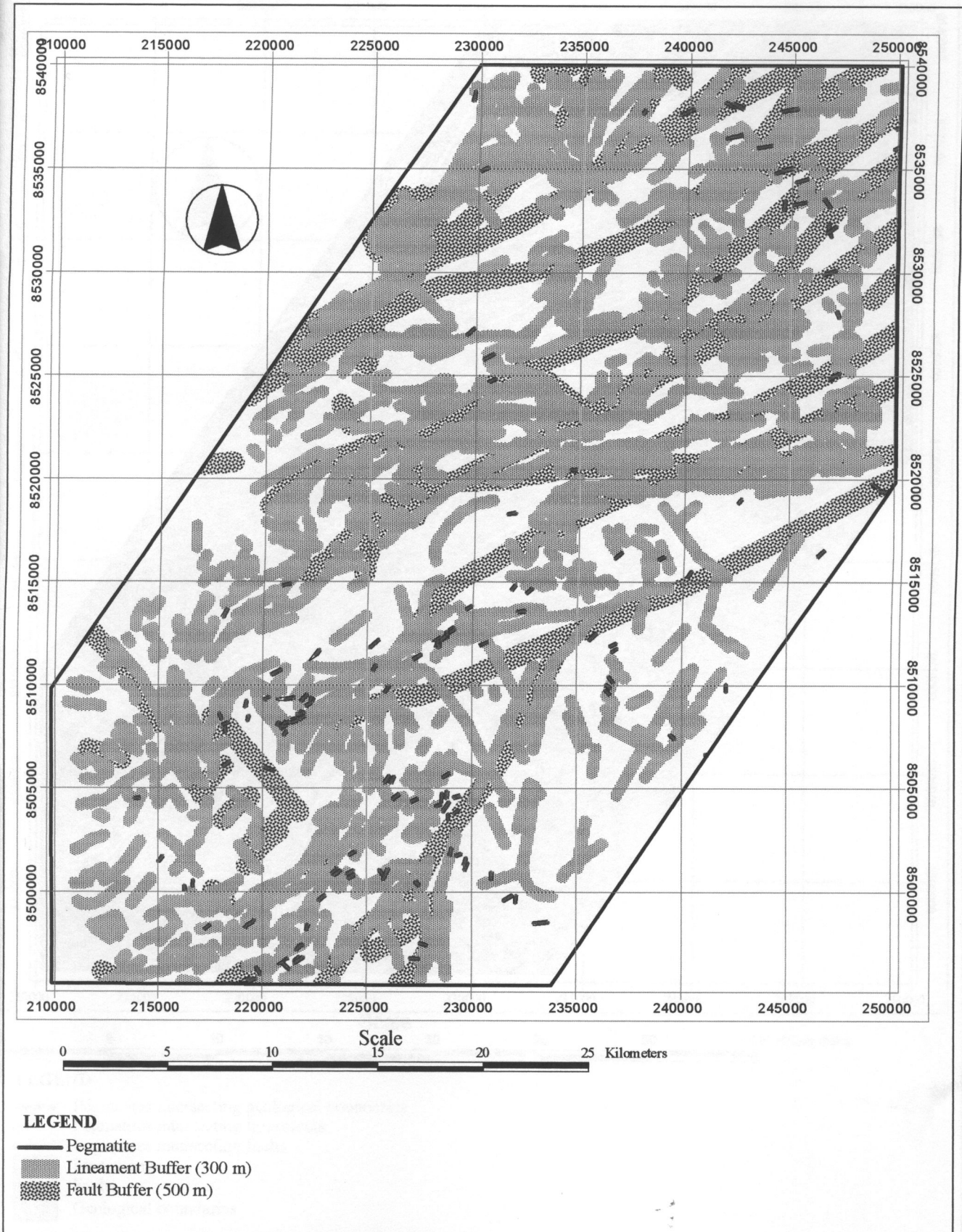


Fig. 6.1: Lineament and fault buffers in the Kaseba-Katota Area

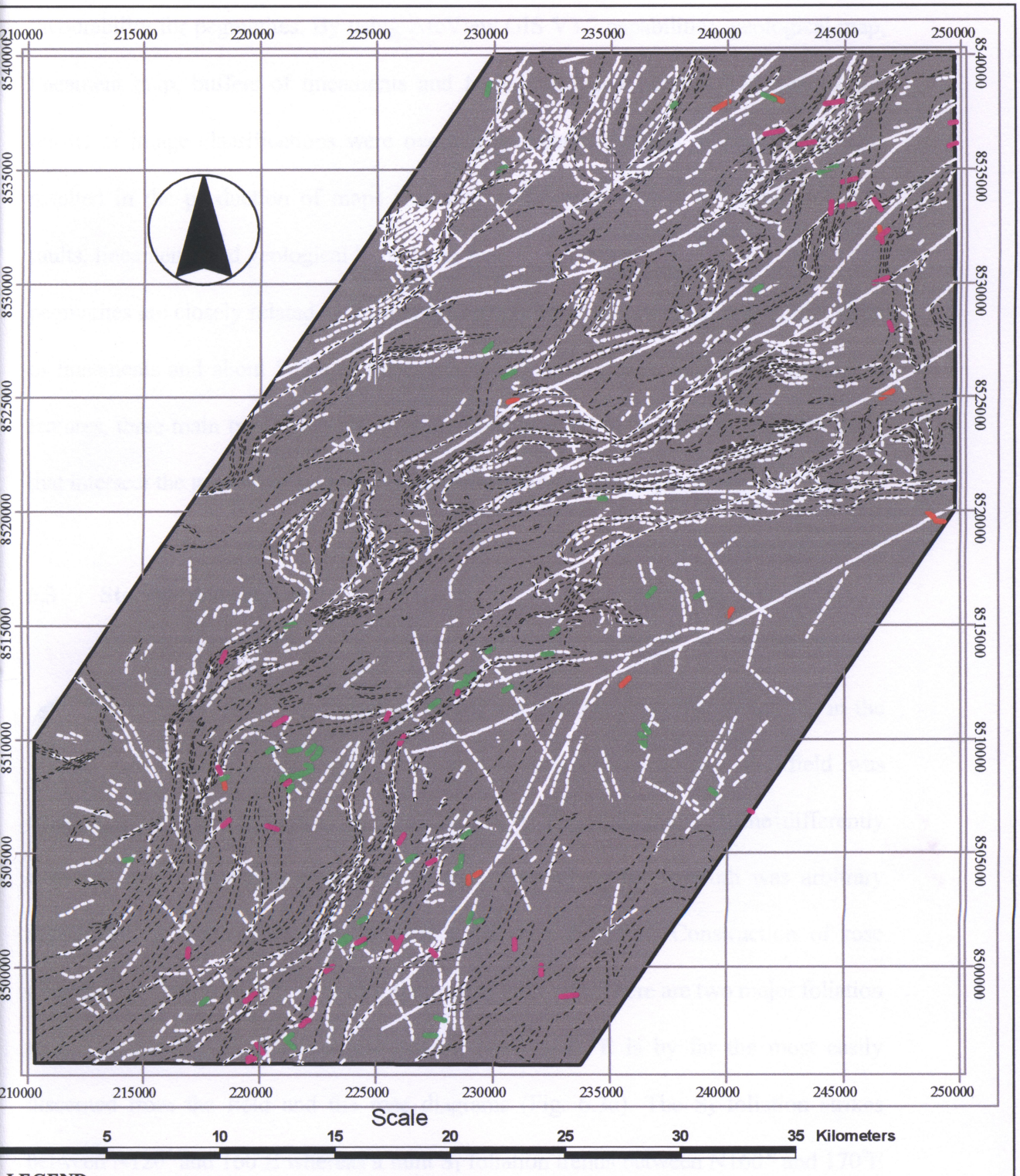


Fig. 6.2: Relationships of Pegmatites with Faults, Lineaments and geological Boundaries

The third stage consisted of combinations of various maps that provide relative favourability for pegmatites. By using ArcView GIS V3.2 capabilities, geological map, lineament map, buffers of lineaments and faults, enhanced Landsat TM images and results of image classifications were overlaid for spatial analysis of pegmatites. This resulted in the production of maps showing spatial relationships of pegmatites with faults, lineaments and geological boundaries (see Figs. 6.1 and 6.2). Fig. 6.1 shows that pegmatites are closely related to lineaments and faults. Most are emplaced within 300m of lineaments and about 500m of the faults. When related to structural and geological features, three main types of pegmatites are distinguished in order of abundance; those that intersect the geological boundaries, lineaments and faults respectively.

## 6.3 Statistical Analysis

One direct way of representing, classifying and analysing the variations in the orientations of geological structure datasets collected from the field was construction of rose diagrams (cf. Woldai, 1995). These diagrams define differently oriented sets of structures (Fig. 6.3). A class interval of $10^{o}$ azimuth was arbitrary applied as the main division to construct the rose diagrams. Construction of rose diagrams was based on the strike of foliation and joint sets. There are two major foliation trends; $S_2$ and $S_3$. The $S_2$ foliation striking N30° to 80°E is by far the most easily discerned from the field and the rose diagrams (Fig. 6.3a). The $S_3$ foliation strikes between N120° and 160°E whereas a faint $S_1$ foliation trends between N160 ° and 170°E (Fig. 6.3b). The prominent set of joints trends N48°E (Fig. 6.3c) and is more or less concordant to the $S_2$ foliation.

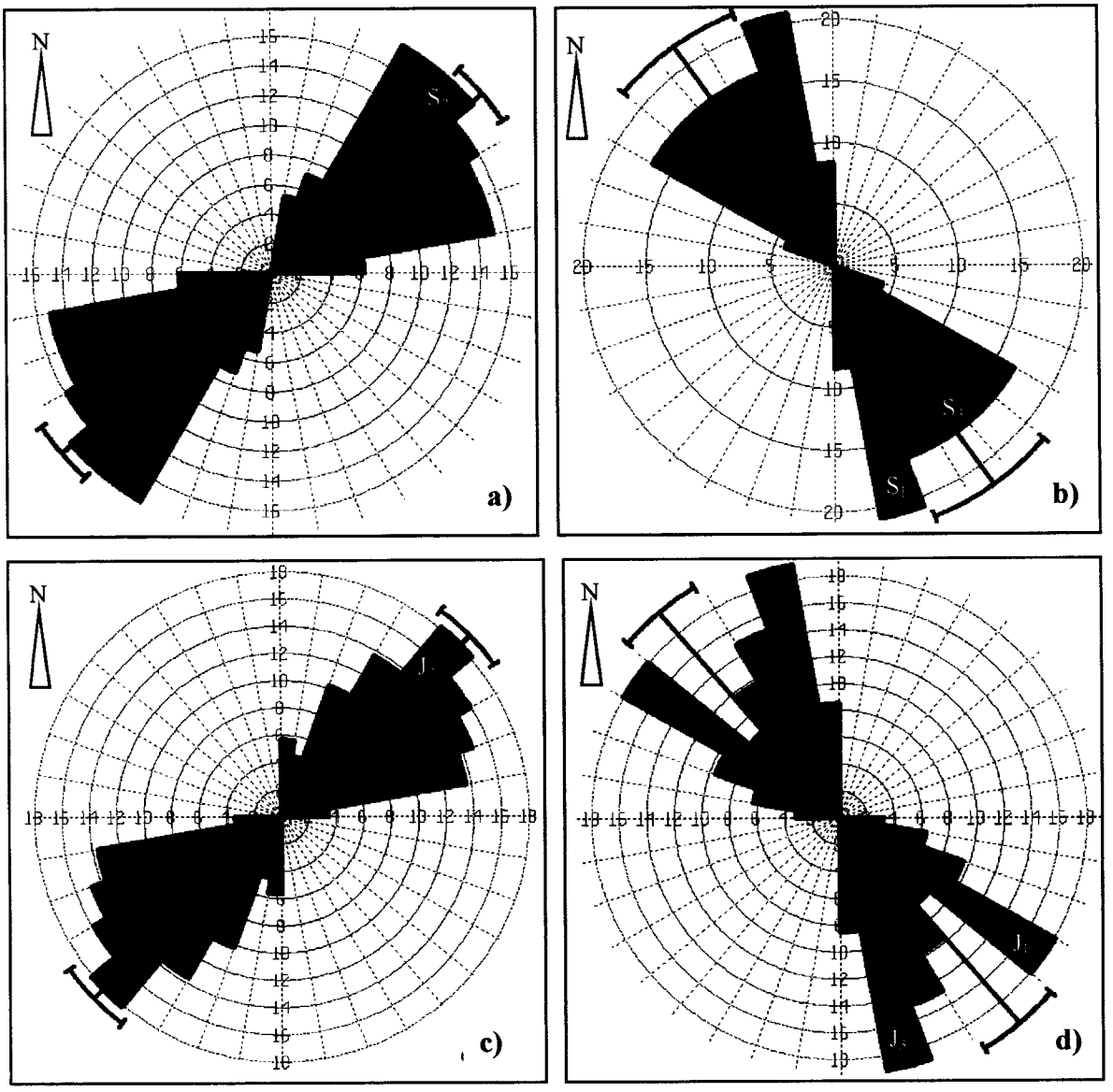


Fig. 6.3: Rose diagrams generated from field measurements. a) Rose diagram of the main $S_2$ foliation in the Kaseba-Katota area. The trend is between N30° and 80°E. b) Rose diagram of $S_3$ foliation with traces of $S_1$ foliation. c) Rose diagram of the major set of $J_2$ joints trending N48°E, in the Kaseba-Katota area. d) Rose diagram of $J_3$ joint set trending N150° - 170°E. Traces of $J_1$ joints strike N130° - 140°E, due to overprinting by $J_3$ joints.

Spatial relationships between the strike of pegmatites, foliation and joints were achieved by matching the rose diagrams of strike of foliation and joints with those of pegmatites (Fig. 6.4). Pegmatites were grouped into four categories as zoned, unzoned, mineralised and barren. Rose diagrams were generated based on the strike measurements of each group. Zoned pegmatites have a general NE trend, and strike between N40° and 70°E (Fig. 6.4a). This matches with the mineralised pegmatites (Fig. 6.4c), the main $S_2$ foliation (see Fig. 6.3a) and the major joint set (see Fig. 6.3c) of rose diagrams.

The spatial distribution of mineralised pegmatites (Fig. 6.5a) was also analysed spatially by "Fry plots". Fry analysis (Fry, 1979) can be operated manually by placing a sheet of paper on which a series of parallel reference lines (north pointing) have been drawn, and the location of each data points recorded. On a second sheet of tracing paper with a centre point (origin), a set of marked parallel lines are kept parallel to those on the first sheet. The origin of the second sheet is placed on one of the data points on the first sheet and the second sheet marked with all the positions of points on the first sheet. This is continued, maintaining the same orientation until all points on the first sheet have been used as the origin on the second. For n data points, there are $n^2-n$ translations. Twenty-four data points were used for the fry plot resulting in 552 data points which brings out a pattern not evident from the initial 24 data points. The resulting Fry plot (Fig. 6.5b) may be analysed by construction of a rose diagram recording the frequency against the direction (cf. Vearncombe, 1998). Although the manual technique provides totally satisfactory answers, the method is tedious and cumbersome even for smaller datasets. Fast and effective analysis can be achieved by the use of advanced software such as SpaDiSTM (Vearncombe, 1998). Fry analysis is of most use in conjunction and as a

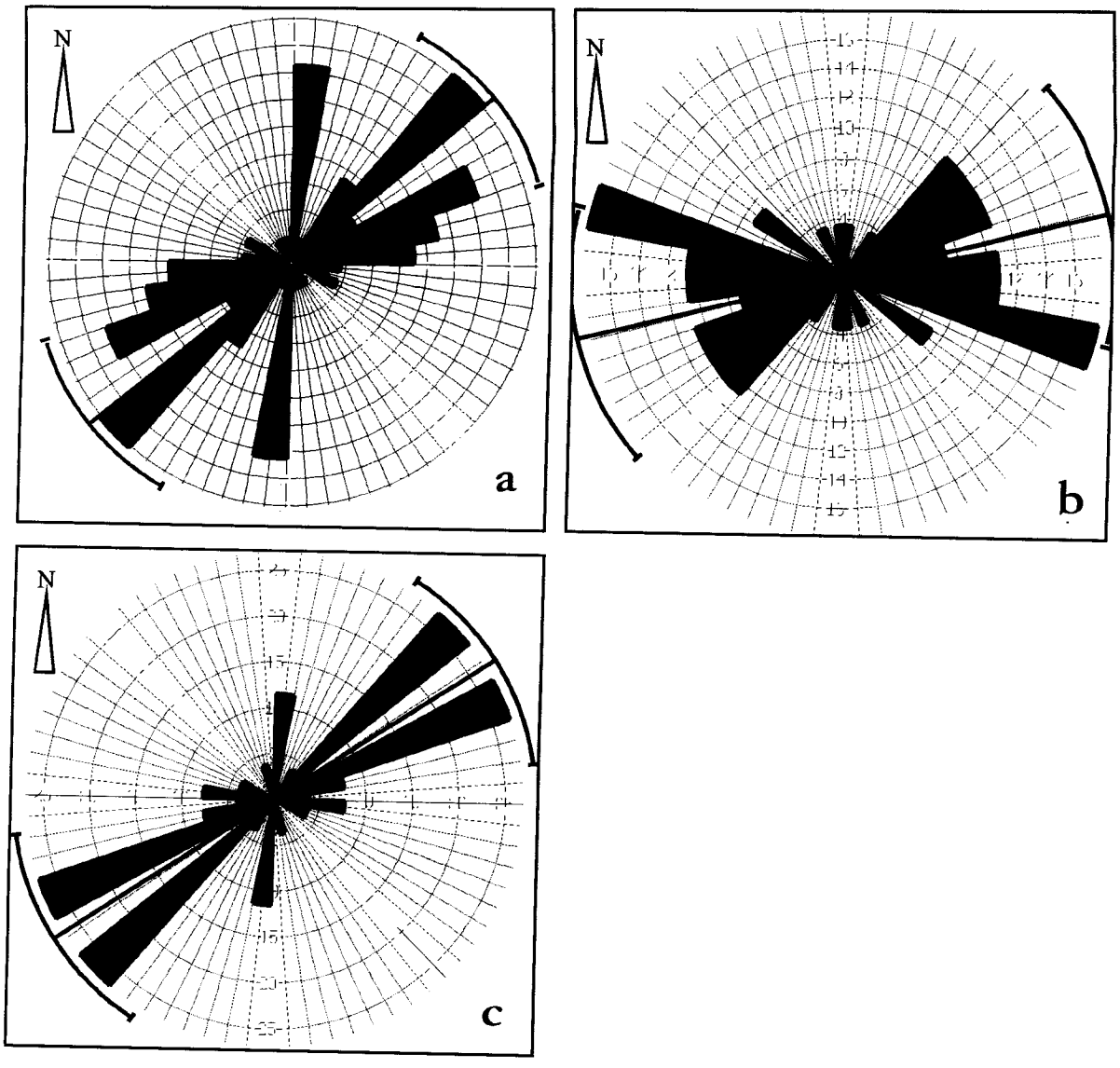


Fig. 6.4: Rose diagrams derived from strike measurements of pegmatites in the field. a) Rose diagram of zoned pegmatites. b) Rose diagram of unzoned pegmatites. c) Rose diagram of mineralised pegmatites (aquamarine, beryl, tourmaline and quartz). The rose diagram of mineralised pegmatites shows a similar trend to that of zoned pegmatites.

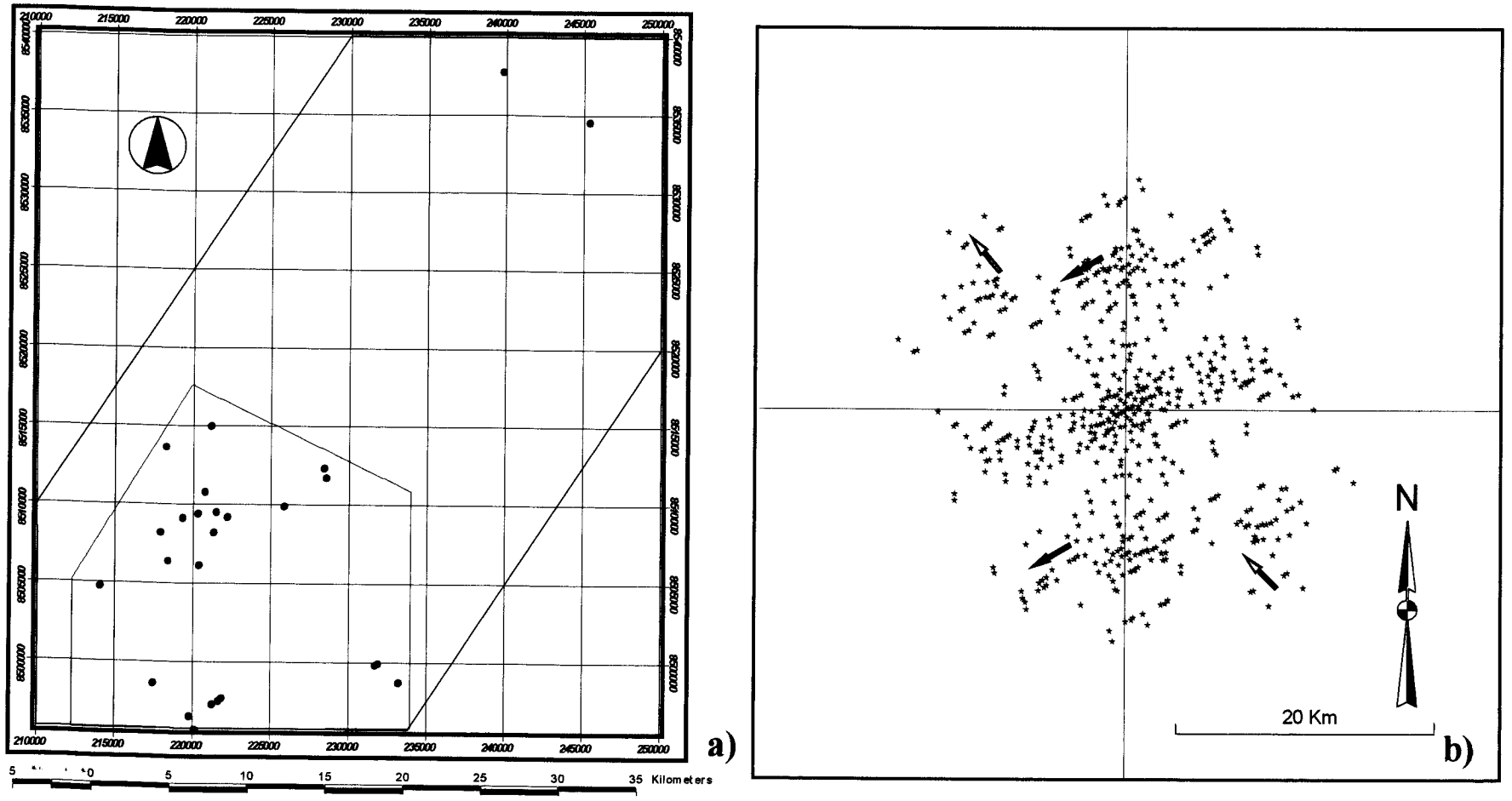


Fig. 6.5: a) Map of Kaseba-Katota area showing locations of mineralised pegmatites. b) Fry plot translated from a selected area of mineralised pegmatites showing prominent trends at 40° to 70° (see black arrows) and subsidiary trends at about 310° and 340° (see white filled arrows).

complement to mapping. The translated data shows a prominent north-east ($40^{o}$ to $70^{o}$) trend and a subsidiary north-west ($310^{o}$ to $340^{o}$) trend of mineralised pegmatites (see Fig. 6.5b). The fry plot brings out the north-west trend which is not noticeable in the rose diagram of the same pegmatites (see Fig. 6.4c).

Statistical analysis has shown a close correlation of the strike and placement of the pegmatites to the strike of major structures (faults, joints and foliation).

# CHAPTER 7

## 7.0 DISCUSSIONS AND CONCEPTUAL MODEL

### 7.1 General

In this study, Landsat TM images and aerial photographs were used for identifying and mapping structural features such as faults and folds, drainage patterns and lithological units. Geologic interpretation of Landsat TM images and aerial photographs over the Kaseba-Katota area was based on the fundamental recognition of elements that include shape, size, pattern, shadow, tone, colour, texture, association and site. Vegetation cover limited recognition and discrimination of these elements in many parts of the study area. In a similar study, Gabert (1990) could not achieve soil and lithologic discrimination due to vegetation cover in the Proterozoic Fold belts of east Central Africa. He only demonstrated the feasibility of lithological discrimination and structural analysis under favourable geological conditions. In an open report, Greenbaum and Amos (1998) found limited applicability of vegetation to geological mapping in their classification of Landsat TM image from Western Desert of Egypt. However, Woldai (1998) achieved lithological discrimination in Sinkat area in Northern Sudan because vegetation is absent. This means that the Landsat TM data that was used, was dominated by solar irradiance and mineralogical effects in soil and rocks, thereby maximising discrimination of lithologies (Woldai, 1998).

In this study, vegetation inhibited the mineralogical effects in the soil and rocks on the Landsat TM image in many areas. To go round this problem, vegetation patterns were used to identify lineaments which are marked by closely spaced trees in areas such as Chitema hills in Fig. 1.1, and shown in detail on the aerial photograph (see Fig. 5.4c). These lineaments represent faults in the Serenje Group (see Fig. 2.1). This phenomenon was used by Allum (1966) in which he referred to alignment of trees or bushes as representing veins, faults, joints and rock boundaries in photogeology and regional mapping. Similar studies were carried out by Nkemba, et. al., (1998) in Solwezi Dome area, in North-western Province of Zambia, which lies in the same geographic region with the Kaseba-Katota area with similar vegetation cover. Vegetation patterns were used in delineating areas with copper mineralisation. Sudden disappearance of vegetation called "copper clearings" identified from the image within thickly forested areas to the north-west of Solwezi Dome was a clue to the presence of concentration of copper mineralisation. Indeed, this study showed that vegetation patterns (and type) could be used in mineral exploration of copper mineralisation whereas the current study used vegetation to map faults, joints, granitic intrusions and metasedimentary ridges in the Kaseba-Katota area.

The continuous trend of outstanding dome- to cone-shaped granite hills of up to 400m long, 200m across and 80m above the ground and their none support of vegetation except for very short grass and scattered shrubs meant easy identification on the Landsat TM image and aerial photographs. Most areas bordering these granites are thickly vegetated resulting in abrupt changes in tonal gradients. The persistent quartzite ridges, which generally rise to 120 m above the plateau level, do not support healthy vegetation.

These are consistent ridges resistant to weathering and erosion and stand out with sharp tonal contrasts on the Landsat image.

The spatial resolution of 28 m x 28 m of the satellite image and vegetation cover in many areas restricted the size of geological features that were identified, to those greater than 3600m$^2$ and structures including pegmatites to those greater than 100m long. However, small-scale satellite (cut-outs) data, supplemented with large-scale aerial photos, was found to be ideal indirect source of information in this study. This was augmented by contrast stretching, edge enhancements and high-frequency filtering through the image and shaded relief models. Similarly, preliminary studies by Nkemba, et al., (1999) in the Kamena-Masola area, south-west of Kaseba-Katota area revealed that, lineaments mapped by remote sensing were actually pegmatite ridges of size 6m high and at least 100m long, emplaced along a fault contact between migmatite and porphyroblastic schist. These structures were easily picked mainly due to absence of vegetation and the sharp contrast of tones between the two lithologies (Nkemba et al., 2000a & b). The difference in tones was due to compositional differences resulting in intermediate tones for schist and darker tones for migmatite (cf. Allum, 1966).

With regard to structural geology, prospectors and mining geologists have long realised that, in many mineral provinces, mining districts such as the Katangan Copperbelt Province (Mendelsohn, 1961) occur along linear trends ranging from tens to hundreds of kilometres (such as the 800 km long Lufilian Arc in North-western Zambia) in length and many deposits have been discovered by exploring along the projections of such trends (cf. Malo, et al., 1992). It is with this understanding that in this study, construction of rose diagrams was based on the strike of foliation and joint sets in the rocks because

the Kaseba-Katota area lies within the so-called Pegmatite Belt, which forms a linear structural trend stretching from Choma-Kalomo Block to the Ubendian Belt (see Fig. 1.2). When these rose diagrams (see Fig. 6.3) were compared with those based on the strike of pegmatites (see Fig. 6.4), it was evident that they follow same trends hence the emplacement of pegmatites was largely influenced by these structures. This relationship was further proved by construction of "Fry plots" (see Fig. 6.5) by translating (see Section 6.3) spatial distribution of selected mineralised pegmatites. Similarly, Rowan and Bowers (1995) interpreted linear features from Landsat TM and aircraft radar images of the Reno, Nevada, quadrangle, in which the features were digitised and analysed statistically to show patterns of orientation and density. When compared with distribution of gold and silver mineralisation, these patterns showed that in most areas the linear patterns were expressions of structural features that controlled the mineralisation.

The evidence obtained from the geological and structural setting has led to the generation of a conceptual model, which shows the tectonic evolution of the study area and emplacement of the pegmatites.

## 7.2 Conceptual Model

The data available now is insufficient to allow a full construction of the model. For example, isotropic dating was only done in adjacent areas. However, an attempt has been made to construct a model based on field observations, petrographic work, remote sensing and spatial relationships (Fig. 7.1). The model summarises the

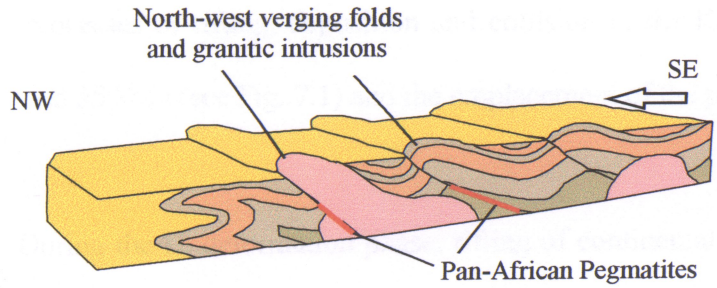


e) Folding, north-west thrusting and post-tectonic magmatic intrusion accompanied by pan-African pegmatitic intrusion around 1000 Ma .

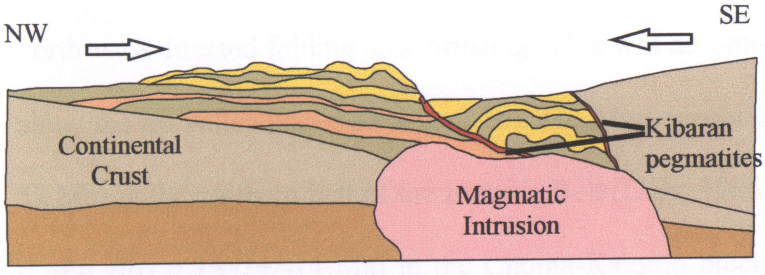


d) Collision, crustal thickening, metamorphism, migmatitisation and syntectonic granitic intrusion at ca. 1100 Ma. Intrusion of (syn-tectonic) Kibaran pegmatites.
Formation of isoclinal $F_1$ folds with northeast trending axial traces, and steeply plunging hinge lines.

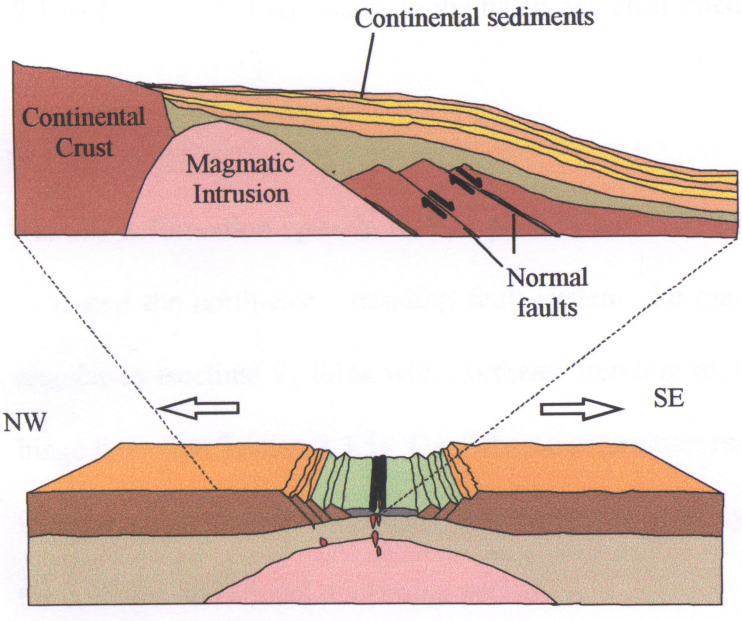


c) Deposition of continental sediments which formed the Serenje Group.

b) Rifting of the continental crust accompanied by magmatic intrusion along the rift valley around 1400 Ma ago.

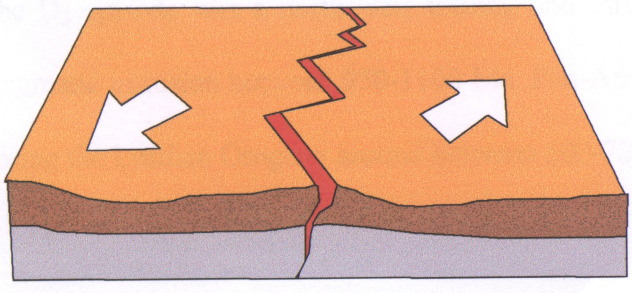

a) Rifting of the continental crust around 1700 Ma.

Fig. 7.1: Block diagrams depicting the conceptual model for the emplacement of pegmatites in the Kaseba-Katota area.

processes of rifting, deposition and collision in the Kaseba-Katota area between 1700 and 550 Ma (see Fig. 7.1) and the emplacement of the pegmatites.

During the $D_1$ deformation phase, rifting of continental crust took place (see Fig. 7.1a). The $D_1$ had its peak at ca. 1355 Ma (Cahen et al., 1984) and is characterised by faint north-west directed folding and thrusting. This was accompanied by magmatic intrusion along the rift valley basin (see Fig. 7.1b). The Mutangoshi Granite (Rb-Sr W. R. 1407+/-39 Ma) in the northern belt of the Irumide Belt (Daly, 1986) and the Siasikabole Granite (U-Pb zircon 1352+/-14 Ma) in the Choma-Kalomo block (Hanson et al., 1988) are a manifestation of this igneous activity. This phase was followed by deposition (see Fig. 7.1c) of continental sediments in the basin, which formed the Serenje Group (see Table 1).

The $D_2$ deformation episode had its peak at ca. 1100 Ma. This period (see Fig. 7.1d) produced the north-east - trending fault system, the main $S_2$ foliation in the area and angular to isoclinal $F_1$ folds with northeast trending axial traces, and steeply plunging hinge lines (see Section 3.3.2). The Kibaran pegmatites mostly rich in aquamarine, beryl, feldspar, mica, tourmaline, quartz and magnetite were syn-tectonically intruded during the collision and crustal thickening period.

The $D_3$ episode was a north-west folding and thrusting associated with post-tectonic magmatic intrusion between 950-1100 Ma. Pan-African pegmatitic intrusion took place during the Lufilian Orogeny around between 500-700 Ma.

From the above description, pegmatites occur within the gneiss-schist-migmatite complexes. Two types of pegmatites are evident on the basis of time of emplacement (Kibaran Vs Pan-African), internal structure and mineralisation.

Kibaran pegmatites (~1100 Ma) are zoned, foliated and strike between $20^{o}$ – $80^{o}$ being parallel to sub-parallel to the main Irumide structures in the host rocks such as faults, main joints and $S_2$ foliation. Cross sections in these pegmatites show at least three zones distinguished on basis of mineralogy, namely the core, intermediate and wall zones. The Kibaran pegmatites host economic minerals such as aquamarine, beryl, feldspar, tourmaline, quartz and magnetite.

The Pan-African pegmatites (~700 Ma) are emplaced obliquely or perpendicularly ($300^{o}$ – $350^{o}$) to the main Irumide trend and to the Kibaran pegmatites. These pegmatites are massive, economically barren and do not show any significant internal structure.

These features and characteristics in the Kibaran and Pan-African pegmatites can be used in mapping of the pegmatites in the Kaseba-Katota area.

CHAPTER

8

# 8 CONCLUSIONS

Conclusions arising from this study can be summarised in the following ways:

The Kaseba-Katota area lies in the Mesoproterozoic intracratonic Irumide belt with a tropical climate and a gently rolling plateau country at about 1,200 m above sea level.

The Kaseba-Katota area is underlain by the Muva Supergroup, which is subdivided into Serenje and Gneiss groups.

Three episodes of deformation associated with metamorphism have led to development of lineaments, faults and folds. Generally, the metamorphic grade in the Kaseba-Katota area increases from greenschist in the northwest to upper amphibolite in the south-east.

Structural domains have been identified according to their orientation, which are considered as of particular importance for pegmatite exploration. These are NE-SW and NW-SE in order of importance respectively.

Mineral resources in the pegmatites, which include aquamarine, beryl, feldspar, mica, tourmaline, quartz and magnetite, are suitable for small- and medium-scale mining and could be a source of employment, income and export earnings.

Extensive field checks have shown that pegmatites commonly occur as lensoids and dykes and occur within the gneiss - schist - migmatite complexes. The pegmatites are concordant to the foliation of the host rocks.

This study has shown that pegmatites are of two generations namely Kibaran age (~1100 Ma) and Pan-African age (~700 Ma). The Kibaran pegmatites are foliated, zoned and strikes between $20^{o}$ – $80^{o}$ and host economically important minerals such as aquamarine, beryl, feldspar, mica, tourmaline, quartz and magnetite. The Pan-African pegmatites are mainly massive, economically barren and emplaced obliquely or perpendicularly to the main Irumide trend.

Satellite images and aerial photographs were interpreted resulting in a dataset consisting of lineaments, faults, folds and lithological units. The image processing and enhancement techniques employed in this study enhanced major structures and continuity of lithologic units such as schists, quartzites and granites. Colour composite images supplemented with image classifications categorised different spectral characteristics corresponding to discrete surface materials such as granitic intrusions (Gneiss Group), pegmatite excavations and metasedimentary ridges (Serenje Group).

Geographic Information Systems (GIS) capabilities were fully employed in this study to integrate, manipulate, analyse, relate and output geological and spatial data generated both by field mapping, satellite and aerial data interpretation. The resulting spatial relationships between the different datasets integrated in the GIS show that the strike and dip of lineaments are consistent with those of pegmatites and that most of the pegmatites

are emplaced within 300m of lineaments. Hence the lineaments must have localized the upward flow of magmatic/hydrothermal fluids.

The conceptual model, shows that collision, crustal thickening, metamorphism, migmatisation and magmatic intrusion at ca. 1100 Ma triggered emplacement of the Kibaran pegmatites, whereas folding, north-west thrusting and post-tectonic magmatic intrusion led to the emplacement of Pan-African pegmatites.

## REFERENCES

**Ackerman E., 1950.** Ein neuer Faltengurtel in Nordrhodesien und seine tectonische Stellung im afrikanischen Grundgebirge. *Geol. Rdsch. p.38-39*

**Allum J. A. E., 1966.** Photogeology and Regional Mapping. *Regional International Library of Science, Technology, Engineering and Social Studies. Robert Maxwell, M. C. 31pp.*

**ARC/INFO V7.1.2, 1997.** Environmental Systems Research Institute, Inc. *380 New York Street, Redlands, California 92373-8100, USA.*

**ArcView GIS V3.2, 2000.** Environmental Systems Research Institute, Inc. *380 New York Street, Redlands, California 92373-8100, USA.*

**Avery T. E. and Berlin G. L., 1985.** Fundamentals of Remote Sensing and Airphoto Interpretation. *Fifth Edition. Prentice Hall. Upper Saddle River, New Jersey 07458. 472pp.*

**Cahen L., Snelling N. L. and Delhal J. R., 1984.** The Geochronology and Evolution of Africa. *Oxford University Press. 215pp.*

**Clive A. B., 1990.** Four Dimensional Analysis of Geological Maps. Techniques of Interpretation. *Department of Geology, University of Southampton. John Wiley & Sons Ltd. 296pp.*

**Cordiner R. J., 1999.** The Geology of the Kanona area: explanation of degree sheet 1330 NE quarter. *Report Geological Survey, Zambia. 54pp.*

**Cvetkovic D., 1973.** Sources of Feldspar in the Serenje and Mita Hills Areas. *Report Geological Survey, Zambia. Economic Report no. 32. 15pp*

**Daly M. C. and Unrug R., 1982.** The Muva Supergroup of Northern Zambia. *Geological Society Special Publication in Episodes Journal of International Geoscience. 266pp.*

**Daly M. C., 1986.** The intra-Cratonic Irumide Belt of Zambia and its bearing on Collision Orogeny during the Proterozoic of Africa. *Collision Tectonics, Geological Society Special Publication in Episodes Journal of International Geoscience Vol.23 No.2 p.128.*

**Fry N., 1979.** Random point distributions and strain measurement in rocks: *Tectonophysics, v. 60, p.1481-1500.*

**Gabert G., 1990.** Geological Application of Remote sensing to African Proterozoic Fold belts and Experiences of the GARS Kibaran Project. *Musee Royal de L'Afrique Centrale – Tervuren, Belgique. Annales – serie in 8° – Sciences Geologiques – n°96 190pp.*

**Greenbaum D. and Amos B. J., 1998.** Remote Sensing and Image Analysis: a practical training guide for Geologists (Revised Edition). *British Geological Survey Technical Report WO/98/01, 245pp.*

**Guernsey T. D., 1951.** A Summary of the Provisional Geological Features of Northern Rhodesia. *Colon. Geol. Min. Resour. 1(1950), p.121-151.*

**Gupta P. R., 1991.** Remote Sensing Geology. Department of Earth Sciences. *University of Roorkee 247 667, India. Springer – Verlag 356pp.*

**Hanson R. E., Wilson T. J., Brueckner H. K., Onstott T. C., Wardlaw M. S., Johns C. C. and Hardcastle K. C., 1988.** Reconnainssance, Geochronology, Tectonothermal Evolution and Regional Significance of the Middle Proterozoic Choma-Kalomo Block, Southern Zambia. *Precambrian Research, p.42, 39-61.*

**Klink B. A., in press.** The Geology of the Chisomo Area, explanation of degree sheet 1330 SE quarter. *Report Geological Survey, Zambia, 78pp.*

**Lavreau J. and Bardinet C., 1988.** Image Analysis, Geological Control and Radiometric Survey of Landsat TM Data in Tanzania. *Musee Royal de L'Afrique Centrale – Tervuren, Belgique. Annales – serie in 8° – Sciences Geologiques – n°96 190pp.*

**Lundén B., Bax G. and Wester K., 1993.** Satellite Imagery and Digital Terrain Model for Studies of Tectonic Structures in Northern Scandinavia. *Remote Sensing*

*Centrale – Tervuren, Belgique. Annales – serie in 8° – Sciences Geologiques – n°96 190pp.*

**Lundén B., Bax G. and Wester K., 1993.** Satellite Imagery and Digital Terrain Model for Studies of Tectonic Structures in Northern Scandinavia. *Remote Sensing Laboratory, department of Physical Geography, Stockholm University, S-106 91 Stockholm, Sweden. 46pp.*

**Malo M., Roy F. and Pelchat C., 1992.** Structurally-controlled mineralisation along the Grand Pabos fault zone, Gaspe Peninsula, Quebec Appalachians. *Geological Association of Canada Annual Meeting, Programme with Abstracts Volume 17, p.73.*

**Mapani B. E. S. and Moore T. A., 1995.** The Geology of the Serenje area, explanation of degree sheet 1330 NW quarter. *Report Geological Survey, Zambia. 51 pp.*

**Mendelsohn F., 1961.** The Geology of the Northern Rhodesian Copperbelt. Roan Antelope Copper Mines Limited. *Acdonald & Co. (Publishers) Ltd. 49-50 Poland Street, London, W.1. 523pp.*

***Nkemba S., De Waele B., and Nyambe I. A., 1998.*** *Application of Geographic* Information Systems (GIS), Digital Data Processing and Remote Sensing Techniques In Mineral Exploration. *Proceedings on the Workshop on Digital Information in Mineral Exploration, 19-23 October 1998, Dar Es Salaam. Geodesa – Esamrdc 26pp.*

**Nkemba S., De Waele B. and Nyambe I. A., 1999.** Pegmatite and Structural mapping using Multiple-source Remotely Sensed data in the Kamena-Masola Area, Serenje District, Central Zambia. *International Geological Correlation Program - IGCP 418/419 (UNESCO/IUGS) Kitwe. Geological Society of Zambia. 4pp.*

**Nkemba S., De Waele B. and Nyambe I. A., 2000a.** Use of TM Satellite Imagery and Aerial Photograph Data in Mapping of Pegmatites and Structures in The Kamena-Masola Area, Serenje District, Central Zambia. *Proceedings on the 28th International Symposium on Remote Sensing of Environment, Cape Town 2000. 4pp.*

**Nkemba S., De Waele B. and Nyambe I. A., 2000b.** Applications of Geographic Information Systems (GIS), Digital Data Processing and Remote Sensing Techniques in Mineral Exploration in the Solwezi Domes area, Northwestern Zambia. *Proceedings on the 28th International Symposium on Remote Rensing of Environment, Cape Town 2000. 4pp.*

**Nyambe I. A., 2000.** Economic, Environmental and Social Impacts of Small-scale Mining. *31st International Geological Congress (IGC), Rio de Janeiro, 2000. August 6-17. 4pp.*

**PCI Image-Works Version 7., 2000**. PCI Geomatics Group. *50 West Wilmot Street, Richmond Hill, Ontario, Canada, L4B 1M5.*

**Rowan L. C. and Bowers T. L., 1995.** Analysis of Linear Features Mapped in Landsat Thematic Mapper and side-looking Airborne Radar Images of the Reno,

Nevada 1° by 2° Quadrangle, Nevada and California-implications for Mineral Resource Studies. *Photogrammetric Engineering and Remote Sensing, v. 61, 749-759pp.*

**Sabins F. F., 1996.** Remote Sensing. Principles and Interpretation. *University of California, Los Angeles. H. W. Freeman and Company. New York. 494pp.*

**Trapnell C. G. and Clotheir J. N., 1957**. The Soils, Vegetation and Agricultural Systems of North-western Rhodesia. *2nd Ed. Lusaka. 146pp.*

**Vearncombe J. R., 1998.** Developments in understanding the geology and exploration potential of southern and eastern Africa. *Australian Institute of Geoscientists Bulletin 25, p.9-16.*

**Vincent R. K., 1997.** Fundamentals of Geological and Environmental Remote Sensing. *Bowling Green State University Prentice Hall, Upper Saddle River, New Jersey 07458. 366pp.*

**Woldai T., 1995.** Lithological and Structural Mapping In a Vegetated Low-Relief Terrain Using Multiple-Source Remotely Sensed Data: A Case Study of The Calañas area in Southwest Spain. *Department of earth resource surveys, ITC. 144pp.*

**Woldai T., 1998**. Landsat Thematic Mapper Data as an Aid to the Geological Mapping of the Sinkat Area, Northern Sudan. *DGPF/E Schweizerbart'sche Verlagsbuchhandlung, D-70176 Stuttgart 285-294pp.*